Magnetic Nanoarchitectures for Cancer Sensing, Imaging and Therapy

Nikola Z. Knezevic,[1] Ivana Gadjanski,[1,2] Jean-Olivier Durand[3]*

1. BioSense Institute, University of Novi Sad, Dr Zorana Djindjica 1, Novi Sad 21000, Serbia

2. Belgrade Metropolitan University, Tadeusa Koscuska 63, 11000 Belgrade, Serbia

3. *Institut Charles Gerhardt Montpellier UMR 5253 CNRS-UM2-ENitcSCM-UM1 CC1701 Equipe Chimie Moleculaire et Organisation du Solide Place Eugene Bataillon, 34095 Montpellier Cedex 05 (France)*

*Corresponding author: Jean-Olivier Durand, durand@univ-montp2.fr

Abstract: The use of magnetic nanoparticles for sensing and theranostics of cancer has grown substantially in the last decade. Since the pioneering works, which reported magnetic nanoparticles for bio-applications more than fifteen years ago, the nanomaterials gained in complexity with different shapes (nanoflowers, nanospheres, nanocubes, nanostars etc.) and constitution (e.g. core-shell) of nanoparticles for an increase of the sensitivity (imaging or sensing) and efficiency through synergistic treatments such as hyperthermia and drug delivery. In this review, we describe recent examples concerning the use of magnetic nanoparticles for bio-applications, from the surface functionalization methods to the development of cancer sensors and nanosystems for magnetic resonance and other imaging methodologies. Multifunctional nanosystems (nanocomposites, core shell nanomaterials) for theranostic applications involving treatments such as hyperthermia, photodynamic therapy, targeted drug delivery, gene silencing are also described. These nanomaterials could be the future of medicine, although their complexity raises concern about their safety.

1. Introduction

Despite a variety of molecular therapeutics for cancer currently being applied in clinics and the promising achievements in this research area,[1,2] serious adverse effects of the molecular cytotoxic agents led to the design of nanoparticulate therapeutics for selective cancer targeting.[3] Several specific properties of nanomaterials enable their use for selective cancer treatment. These characteristics include: a) their size, which leads to preferential accumulation of nanoparticles (NP) in tumors through the leaky vasculature of cancer, i.e enhanced permeability and retention (EPR) effect;[4] b) high surface area to attach different molecular therapeutics and c) possibility to functionalize the surface with cancer-homing ligands to further enhance their cancer targeting property. In case of using magnetic nanoparticles (MNP), all these advantages are further supplemented with possibilities for sensing and imaging through external magnetic field-related measurements and for enhanced targeting through exposure to disease-localized magnetic force. Superparamagnetic iron oxide nanoparticles (SPION) are most widely used type of MNPs, which is typically magnetite (Fe_3O_4), with monodomain particles in the size range of about 5–20 nm and characterized by high magnetic saturation and high biocompatibility. High potential of SPION for biomedical applications is being demonstrated in scientific literature for quite some time,[5] and certain formulations of surface coated magnetite-based nanotherapetics already gained the U S Food and Drug Administration (FDA) approval for use in humans as iron deficiency therapeutics and as magnetic resonance imaging (MRI) contrast agents (e.g. Feraheme®, Feridex I.V.®, and Gastromark®).[6]

The recent research developments have progressesed towards more elaborated and complex multifunctional magnetic designs. This multifunctionality reflects in achieving several functions at the same time, such as simultaneous cancer targeting, imaging and therapy.[7]

The concept of applying MNPs for cancer sensing is based on the selective interaction between functionalized MNP and the cancer-specific biomolecule or cancer cell, typically through specific antibody-antigen interactions, which leads to the change in measured magnetic property of the nanoparticle. MNPs also enable MRI of the tissues by acting as contrast agents. While SPION typically acts as a contrast agent by shortening the T2 relaxation times of the nearby nuclei, other magnetic nanomaterials are being increasingly developed for acting as T1-contrast agents.[8] Contrast agents functioning by shortening T1 are considered as "positive" contrast agents, giving a bright signal for the surrounding tissue, which is beneficial for increasing the resolution of the imaging. However, "negative", darkening T2 contrast agents typically do not require short proximity between the nuclei and the contrast agents, as in the case of T1 agents, which can be highly useful for achieving selective imaging, e.g. for detection of brain metastases by MRI with antibody-functionalized microparticles of iron oxide as the T2 contrast agent.[9] Different therapeutic approaches are available through application of MNPs, which may include magnetic-field responsive drug delivery, hyperthermia or both processes at the same time for the synergistic effect against cancer.

Hence, the magnetic nanomaterials exhibit high potential for clinical applications in targeted treatment of diseased tissues and simultaneous MRI for monitoring the treatment. Synthesis, functionalization strategies and different application potentials of SPION were reviewed in detail in the literature.[10–12] Reviews focusing on theranostics with magnetic nanomaterials,[13–20] and studies detailing the research contributions in magnetic mesoporous silica nanoparticle (MMSN)-based multifunctional systems[21,22] were also reported. In the current review article, we focus on

recent, most relevant functionalization strategies of multifunctional, multicore, MNPs and their demonstrated application potentials for cancer sensing, imaging and therapy (Figure 1).

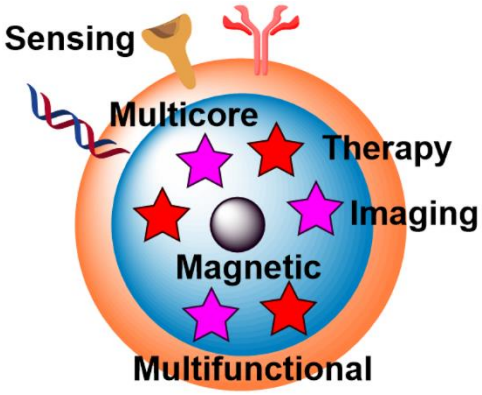

Figure 1. Schematic representation of a general approach for devising multifunctional magnetic nanoparticle containing different layers, i.e. core magnetic NP, middle layer containing different therapeutic (red stars) and imaging agents (purple stars) and outer layer containing different functional groups (peptides, antibodies, aptamers) for targeting the tumor tissues, for achieving simultaneous sensing, imaging and therapy.

2. Functionalization of magnetic nanoparticles

Direct attachment of desired molecules to the surface of MNPs is often possible due to the presence of electrophilic metal ions or nucleophilic anions on their surface. However, in case of insufficient affinity for the nanoparticle surface, functionalization with the desired molecules is achieved through different sequential linking strategies. The attachment of the linker to the molecule may be initially achieved in solution through a homogeneous reaction, followed by a heterogeneous reaction where such a newly formed conjugate is grafted to the surface of the nanoparticle. On the other hand, the desired functionalized nanoparticle may be built in sequence, through sequential

heterogeneous reactions of MNPs with the linker, followed by conjugation with the desired molecule.

Employment of homogeneous reactions is certainly preferred as much as possible due to higher reaction yields. However, the methodology with sequential heterogeneous reactions is often favored because of the facile separation of the products from byproducts through filtration, centrifugation or magnetic separation. Hence, this methodology may be useful in case of multicomponent functionalization reactions, in the presence of catalysts, or in the case of difficulties in separation of surface-reactive side product after the homogeneous couplings. On the other hand, in case where catalytic molecules and byproducts of the homogenous coupling processes are not reactive with the nanomaterial's surface it may be desirable to perform *in situ* functionalization of nanomaterials with linker-modified molecules immediately after the homogeneous coupling reaction, and hence to remove all of the soluble side-products and catalysts by a single separation of the final functionalized material.

Nanomaterials which contain hydroxylated surfaces of metal ions (Fe, Al, Ti) or silicon (e.g. Fe_3O_4, Al_2O_3, TiO_2, mesoporous silica nanoparticles (MSN)) can be functionalized with silicon-based bifunctional reagents.[23–26] Various commercially available alkoxysilanes can be grafted on the surface of these nanoparticles, to introduce different functional groups (thiol, amine, halide), which are useful in subsequent conjugations. The grafting process is usually performed in dry solvents at an elevated temperature, in order to promote the formation of covalent linkage between nucleophilic surface hydroxyls and the reagent's electrophilic Si atoms. This reaction is possible even in the presence of water, though various side reactions are promoted in these conditions through hydrolysis of organosilane reagents and hence their homologous couplings. As an example, covalent functionalization of genomic DNA to magnetic nanoparticles was recently reported.[27]

Initial functionalization of the magnetite surface was investigated through two pathways, and both utilize silanization procedures with organosilane reagents. In case of using N-(2-aminoethyl)-3-aminopropyltrimethoxysilane for surface functionalization (Figure 2), the chelating diamine functionality was further reacted with potassium tetrachloroplatinate to create an analog of cisplatin on the surface and thus enable attachment of DNA to platinum through guanine bases. The second approach involved silanization of the surface with 4-aminobutyltriethoxysilane, where subsequent alkylation with tris(2-chloroethyl)amine hydrochloride yielded an analogue of nitrogen mustard chemotherapy agents on the surface, which was capable to bind covalently to the genomic DNA. The prepared DNA-functionalized MNPs were demonstrated for application in removing the excess chemotherapy agents (doxorubicin, cisplatin, and epirubicin) from biological solutions.

Besides hydroxyl groups, magnetic iron-oxide and other metal-based nanoparticles may also contain surface-metal ions. This type of surface is typically functionalized with bifunctionalized ligands, where one of the functional groups is a metal-coordinating group while the other functional group has weaker affinity for metal-coordination and remains free for further modification. Thus, magnetic iron-oxide nanoparticles could be functionalized through carboxylate[28] or phosphonate coordination.[29] Phosphonate coordination is increasingly used and has been recently shown to be very efficient for surface modification of iron oxide nanoparticles. Indeed, attachment of cytochrome P450 BM3 enzyme that contains both monooxygenase and reductase domains to magnetic nanoparticles was achieved through the usage of phosphonate bifunctionalized ligand N-phosphonomethyl iminodiacetic acid ((PMIDA), Figure 2).[30] Attachment of PMIDA to the surface of magnetite nanoparticles occurs through the phosphonate group, leaving the carboxylate moieties for further reaction. In this study, coordination of Ni^{2+} ions to the carboxylates was first employed, followed by the coordination of the histidine tag of the enzyme to the remaining coordination sites

of Ni^{2+}. Increased stability and prolonged activity of the magnetite-functionalized enzyme was also achieved through cross-linking the enzyme with glutaraldehyde.

Recent article investigated functionalization of piezoelectric/ferroelectric bismuth ferrite (BiFeO3, BFO) films and particles with bifunctional ligands benzene-1,4-dicarboxylic acid (BDC) or with the phosphonobenzoic acid (PBA, Figure 2), after a pre-activation step with hydrogen peroxide (H_2O_2) to produce -OH groups on the surface.[31] The authors concluded that in case of PBA the surface functionalization occurred preferentially through the phosphonate group. In case of BDC as the ligand, the functionalization was also successful though a significant portion of BDC molecules was lying down parallel to the surface with both carboxylic terminations deprotonated and attached to the surface. In another study, Sandre and co-workers synthesized multifunctionalized iron oxide nanoparticles and nanoflowers.[32] The surface functionalization of the nano-objects with PEG groups and the near-infrared fluorescent probe DY700 was carried out in one step through a very efficient convergent strategy using phosphonate anchors. The nanoflowers were demonstrated to be more efficient than single core nanoparticles for the destruction of cancer glioblastoma cells through magnetic hyperthermia, leading to 80-90% of cell death.

Functionalization of cell penetrating peptides (CPP) on MNPs was recently investigated to enhance the lysosomal escape and cell uptake of the nanoparticles. One of the strategies for functionalization of SPION,[33] obtained using the Massart protocol,[34] with cyanine fluorescent dye emitting in far red, polyethylene glycol (PEG5000) coating, and the membranotropic peptide gH625, involved initial functionalization of the magnetite surface with 3-aminopropyltrimethoxy silane (APTES), followed by subsequent dicyclohexylcarbodiimide–n-hydroxysuccinimide (DCC–NHS) and thiol-maleimide coupling. In a different functionalization approach, the initial

surface functionalization was achieved by reaction with phosphonate moiety from 3-aminopropylphosphonic acid (Figure 2), and the free amine moiety was further involved for DCC-NHS coupling with folic acid, PEG and gH625 peptide.[35] In both cases the increased cell uptake of CPP-functionalized magnetic nanoparticles was demonstrated by *in vitro* experiments.

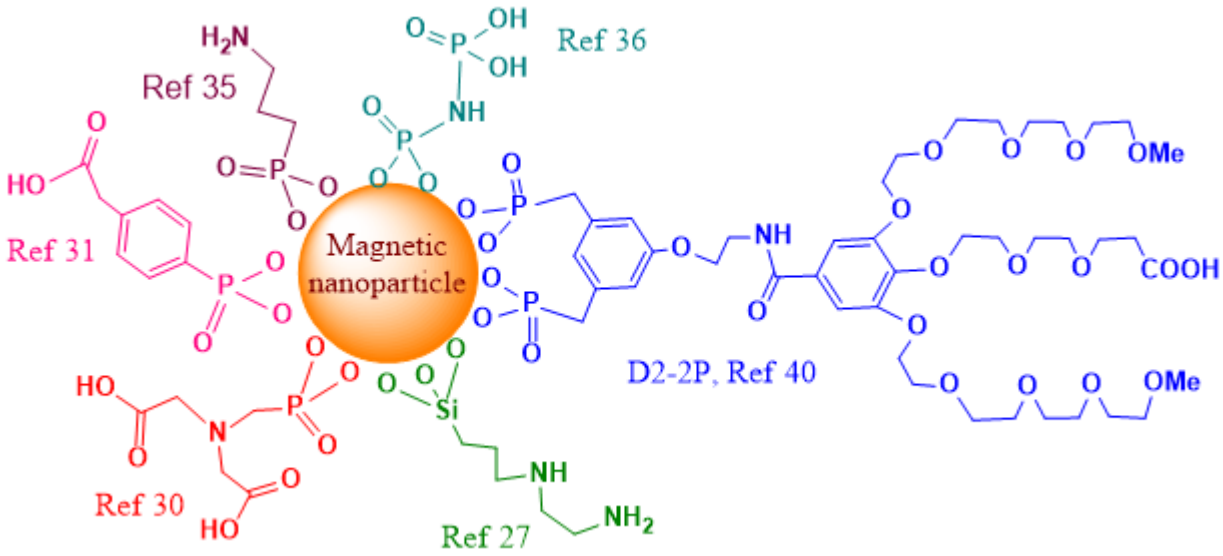

Figure 2. Schematic representation of different surface functionalizations of magnetic nanoparticles

Radiolabeling of magnetite nanoparticles with ^{90}Y, a high energy β-emitter, was recently demonstrated for potential applications in magnetic field-guided delivery of radionuclides to the tumor and imaging.[36] The attachment of the radionuclide was enabled through coordination to phosphonate groups, by surface functionalization of magnetite with multiphosphonate ligands imidodiphosphate (IDP, Figure 2) and inositol hexaphosphate (IHP).

Strong coordination of phosphonate group to Gd^{3+} was utilized to construct renal clearable peptide-$NaGdF_4$ nanodots with active tumor targeting.[37] Functionalization with cell penetrating peptide (CPP), phosphorylated cytosol-localizing internalization peptide 6 (pCLIP6), and phosphorylated

retro-inverso tumor-affinity peptide (pD-SP5) (pD-SP5), was achieved through ligand exchange with oleate on the surface of $NaGdF_4$ nanodots. *In vitro* and *in vivo* experiments revealed that the functionalized nanodots have low toxicity and allow excellent MR imaging of orthotopic colorectal tumor at low dose of the contrast agent. High affinity of Fe^{3+} ions to phosphonate ligands was previously utilized to functionalize the MNPs with different sugars, through ligand exchange of surface oleates.[38]

The similar principle of exchange with phosphonate ligands was recently used to covert hydrophobic iron nanoparticles into water-soluble iron-iron oxide core-shell nanoparticles.[39] The nanoparticles contain monocrystalline body-centered cubic iron core of ca. 10 nm in size surrounded by a spinel oxide shell of ca. 2 nm thickness, having promising magnetization (156 A m^2 kg_{Fe}^{-1}) and relaxivity (r2 = 335 $mM^{-1}s^{-1}$) values for biomedical applications.

Ligands of oligoethylene glycol dendron structure, containing phosphonic anchor (D2) or a biphosphonic tweezer (D2-2P, Figure 2) moiety were functionalized by the ligand exchange methodology on superparamagnetic spherical iron oxide nanoparticles of 10 nm in diameter, synthesized by thermal decomposition.[40] *In vivo* MRI studies on mice, upon intravenous injections, showed high contrast enhancement and evidences for continuous renal and hepatobiliary excretions of both dendronized NPs, with no signs of toxicity during the period of the experiment (48 h). Particularly interesting is the observation that the D2-2P-functionalized magnetic nanoparticle showed no uptake in three different cancer cell lines, which would be beneficial for devising safe early cancer diagnosis and imaging agents, or for achieving specific active targeting through additional functionalization with targeting ligands.

Polyelectrolytes having different iron oxide complexing units (carboxylic vs phosphonic acid), along with different structure and properties have been investigated for direct functionalization of

the surface of magnetofluorescent nanostructures, which are multimodal imaging agents facilitating high resolution diagnosis.[41] As determined, using comblike polyelectrolytes containing carboxylate units, ($n \approx 25$ repetitive units) based on poly(methyl methacrylate), led to the highest colloidal stability of magnetofluorescent nanostructures in aqueous environment. However, application of polyelectrolytes with phosphonic acid moieties lead to disruption of magnetofluorescent nanostructures presumably due to strong interaction of phosphonates with Fe^{3+} ions on the surface, leading to separation of magnetic nanoparticles from the original organic fluorescent framework.

Other research studies also determined that the surface-functionalized molecules can exert an effect on magnetic properties of the nanoparticles.[42–44]

Further modification of the surface of iron oxide nanosystems can be performed through many different chemical conjugation strategies, which have been reviewed in detail.[45,46] Thus obtained multifunctionalized nanoparticles have been showcased for stimuli-responsive therapy and diagnostics of cancer,[47] as well as for image-guided targeted therapy.[48]

3. Application of magnetic nanoarchitectures for cancer sensing and imaging

Magnetic biosensors are being increasingly investigated in the context of cancer nanotheranostics. The key approach is the use of magnetic micro/nanoparticles or magnetic nanostructures coupled to the molecular recognition elements (bioreceptors) such as antibodies, aptamers, DNA probes, small peptides, bacteriophages. The biofunctionalized magnetic nanoparticles (BMNPs) produce the stray field when magnetized by an externally applied field, which provides the signal detectable by the magnetic sensors. The concentration of the BMNPs bound to the analyte is proportional to

the analyte concentration. Many conventional assays that were using fluorescent labeling have been adapted for magnetic sensing using BMNPs, e.g. magnetic immunoassay (MIA).[49,50] Some of the main advantages of magnetic sensing are high sensitivity, high signal-to-noise ratio (SNR), detectability of MNPs in colored mediums and opaque structures, as well as the possibility of using a convenient option for manipulation of the magnetically labeled entities within the microfluidic channels of the sensing device, using externally applied high gradient magnetic fields. Kokkinis et al. harnessed this option to produce microfluidic platform containing integrated magnetic sensors for counting the cancer cells pre-isolated from the whole blood samples.[51] The innovative aspect of the proposed cell chip is that it utilizes BMNPs to label and separate the cancer cells using integrated conducting microstructures. Magnetically labeled and separated cancer cells can be subjected to further complex analyses, which renders described chip a very useful low-cost tool that has potential to simplify workflow in the clinical setting.

Another characteristic potentially useful in a clinical setting is the reusability of the MNPs, as after collecting the BMNPs from the mixed system by an external magnetic field, the captured biomolecules can be washed out, allowing reuse of the magnetic particles.[52] Nevertheless, there is still a number of technical challenges to solve, particularly regarding separation of bound biomolecules, in order to achieve full BNMP recyclability.

In contrast to sensing with fluorescent labels, magnetic biosensing does not face the problem of background noise, since there is no detectable magnetic content in the biological samples, which enables development of the sensing systems with low limit of detection (LOD). However, there are a few disadvantages to the use of BMNPs as well, such as their stability, with respect to the surrounding environment, especially when considering nanoparticles below 100 nm.[53] These disadvantages might be overcome with new developments in the surface functionalization methods.

Another issue when using such small particles that exhibit small magnetic moment is the need for more sensitive measurement systems and sensors, which is another technical challenge for the magnetic biosensing field.

In terms of detection of the magnetic signal, most current applications in life sciences use the magnetoresistance effect. In biosensing applications several different magnetoresistance sensor technologies (giant magnetoresistive, spin valves, and tunnel magnetoresistive) are used, presented in detail in the recently published perspective article by Giouroudi and Hristoforou.[54]

However, a particularly interesting approach for detecting the magnetic signal was developed by Nikitin et al, who use magnetic particle quantification (MPQ) based on the non-linear magnetization of MNPs subjected to an alternating magnetic field at AC frequencies f1 and f2, and subsequently recording the MNP response at a combinatorial frequency f = f1+ f2. MPQ approach is robust and permits registration of minute magnetic signals in the presence of strong noise, providing high sensitivity and precision.[55,56] The Nikitin group developed several MPQ based platforms for quantitative multiplex magnetic immunoassays for different cancer markers, such as prostate-specific antigen (PSA), using the 50 nm or 100 nm superparamagnetic microspheres conjugated to antibodies. The platforms include a) one-run tests on 3D porous filters where the signal was read out from the entire volume of the nontransparent 3D fiber filters employed as solid phase for sandwich immunoassays, with LOD of 12 pg/ml and the dynamic range exceeding 3 orders of concentration; b) disposable flat and micropillar biomagnetic sensor chips where the capture antibodies are placed in several recognition spots on the chip. The target molecule binds to the capture antibodies and subsequently the immunosandwich structure is formed between the captured target molecule and the magnetic label functionalized with the antibody specific for the target molecule, with LOD of 90–100 pg/ml for PSA; c) a lateral flow assay (LFA) test strip with

several test lines with magnetic signals simultaneously recorded from each line independently using a multichannel MPQ reader. This design brings the problem of cross-reactivity of different immunoreagents and BMNPs since they are all simultaneously present in solution and can potentially interact with each other. This problem is reduced with the fourth platform of magnetic biosensors based on a 3D modular architecture where several spatially separated LFA test strips of different specificity are used and simultaneous volumetric detection of MNP from all recognition zones was performed. Described platforms are useful for rapid, simple, sensitive quantitative measurements of different cancer markers and other small molecules.[57]

Immunomagnetic nanosensors are a useful tool not only for quantitative detection but for imaging of cancer stem cells (CSCs) as well. Wang et al. developed the nanosensor for real-time molecular imaging of targeted glioblastoma CSCs, that harnesses specific interaction between cell-membrane marker antigen CD133 of glioblastoma CSCs and anti-CD133 monoclonal antibody (mAb) coupled to MNPs.[50] Superparamagnetic γ-Fe_2O_3 iron oxide nanoparticles were fabricated as nanosensor cores with approximately 10-15 nm in size, and coated with carboxymethyl chitosan via sodium tripolyphosphate crosslinking, and then chemically modified with polyethylenimine (PEI). Anti-CD133 mAb was conjugated to the PEI- MNPs using coupling reagents sulfosuccinimidyl-4-(N-maleimidomethyl)-cyclohexane-1-carboxylate and Traut's Reagent. Formed anti-CD133 mAb-conjugated-MNPs were tested *in vitro* for cell toxicity, specificity and effect on the cell cycle and subsequently delivered to the cultured human brain glioblastoma CSCs for fluorescence imaging and MRI. The mAb-MNP conjugate used for fluorescence imaging was additionally coupled to the rhodamine B isothiocyanate (RBITC) fluorescent probe. Nanosensor particles showed high biocompatibility, specificity and no toxicity. Glioblastoma CSCs targeted with the mAb-MNP conjugate displayed strong fluorescence signal and negative MRI contrast

enhancement (signal darkening) in T2-weighted MRI in comparison to the cells treated with non-mAb-functionalized MNPs, leading to conclusion that described immunomagnetic sensor has high potential for the use as a fluorescence nanoprobe and MR contrast agent for glioblastoma CSC real-time monitoring. However, additional evaluations are needed to confirm the sensor's *in vivo* usability.

Nebu et al. used a different approach to ensure targeting of the biofunctionalized MNPs - BMNPs to the cells while achieving the theranostic effect in parallel.[58] They conjugated MNPs to erlotinib, clinically approved as the efficient inhibitor of epidermal growth factor receptor (EGFR) that is commonly over-expressed by the pancreatic cancer cells (PCCs).[59] Firstly, superparamagnetic Fe_3O_4 cores were produced having gold nanoclusters (AuNC) adsorbed on the surface through electrostatic attraction. The rationale for adding the luminescent AuNC to MNPs is based on the good photo-stability of AuNCs, their ultrafine size, large Stokes shift, size-dependent optical properties and good biocompatibility.[60] Thus formed Fe_3O_4@AuNCs with negatively charged shell were then conjugated to the positively charged erlotinib by electrostatic attraction. The *in vitro* drug release study of erlotinib was done in PBS buffers mimicking two physiological environments with pH = 7.4 and 5.0 at 37°C, evidencing clear enhancement of drug delivery at lower pH values, which is characteristic for cancer tissues. The erlotinib-functionalized MNP-AuNC nanoprobe provided fluorescence enhancement in the confocal microscopy of the cultured PCCs (PANC-1 cell line). Taken together, these results indicate good potential of described anticancer drug-MNP-gold cluster nanoprobe for both imaging (MRI or optical) and drug delivery, two criteria crucial for efficient nanotheranostics.

General tendency in the field of biosensors is to reduce costs of production and to simplify their use for achieving low-cost point-of-care (POC) usability. One of the attempts with regards to POC

cancer diagnostics is described by Tian et al. who devised a microRNA detection biosensor based on combining MNP assemblies with DNAzyme-assisted target recycling, which can lower costs of sensor production in comparison to the protein-enzyme based microRNA detection methods.[61] MicroRNAs are regarded as one of the crucial developments in cancer biology in recent years, with high potential of circulating microRNA to be used as cancer biomarkers, even providing specific microRNA signature for specific cancer types, prognosis and response.[62] Bioresponsive DNA-based scaffolds possess several characteristics such as controllable length, specific hybridization and reactivity with enzymes, which make them a good choice for the use in nanotheranostics, in combination with nanoparticle assemblies, particularly since production of functional DNA sequences such as deoxyribozymes (DNAzymes), aptamers and aptazymes has been improved by the use of SELEX (systematic evolution of ligands by exponential enrichment) technology.[63] DNAzymes – DNA enzymes or catalytic DNA, are single stranded DNA oligonucleotides with nuclease- or peroxidase-mimicking activity, used frequently in combination with nanoparticles as biosensors, particularly for amplified sensing and as proofreading units, especially as multi-component DNAzymes (MNAzymes).[64,65]

Tian et al. devised an interesting concept by using MNP assemblies in combination with DNA scaffolds that also comprise substrate sequences for DNAzyme.[61] When target DNA or microRNA sequences are present, DNAzyme will react with them, catalyzing the cleavage that will further cause the rupture of the scaffolds and disintegration of the MNP assemblies. The number of released MNPs, proportional to the concentration of the target, is quantified by a 405 nm laser-based optomagnetic sensor. Importantly, nucleic acid target sequences are not destroyed during the cleavage reaction, meaning they can be released further to the suspension to induce digestion of multiple DNA scaffolds. The diffusion time for target recycling can be optimized i.e. reduced by

increasing the concentration of the substrate sequences in the MNP assemblies. Interesting aspect of this study is that the MNPs were employed for multiple functions - as labels, carriers and building blocks. Proposed biosensor was tested with short (app. 20 nucleotides) single-stranded DNA and RNA targets and showed limit of detection (LOD) of 1.5 pM target DNA in buffer and LOD of 6 pM target microRNA in 10% fetal bovine serum. However, further studies are needed to confirm the efficacy of described biosensor with cancer-specific microRNA sequences. In addition, further technical optimization is needed, since the current sensor performance is heavily dependent on experimental conditions, such as reaction temperature and reaction time – DNAzymes start denaturization at temperatures higher than 50 °C, while the signal intensity and subsequently sensor sensitivity depends on the reaction time – it is necessary to provide at least 30min long interval as reaction time for the described biosensor.

Circulating tumor cells (CTCs), considered as a valuable biomarker for early cancer detection, are released from primary and metastatic tumors into the bloodstream. Recent report demonstrated application of magnetic mesoporous silica nanoparticle (MMSN) type of material, functionalized with anti-MUC1 aptamer for selective interaction with mucin 1 protein (MUC1) which is over-expressed in more than 90% of human breast carcinomas, to capture CTC from the bloodstream (Figure 3).[66] The amount of the breast cancer cells was quantified by additional specific reaction between overexpressed folate receptors on CTC and the fluorescent probe (FA-BSA-FITC), prepared by linking folic acid and Fluorescein isothiocyanate (FITC) to Bovine serum albumin (BSA). Hence, CTC cells are sandwiched between the fluorescent probe and the AntiMUC1-MMSN, which are isolated from the sample by magnet and further quantified by fluorescence. The constructed detection system showed excellent selectivity in the presence of different cell lines, good reproducibility and accuracy, with LOD of 100 cells/mL.

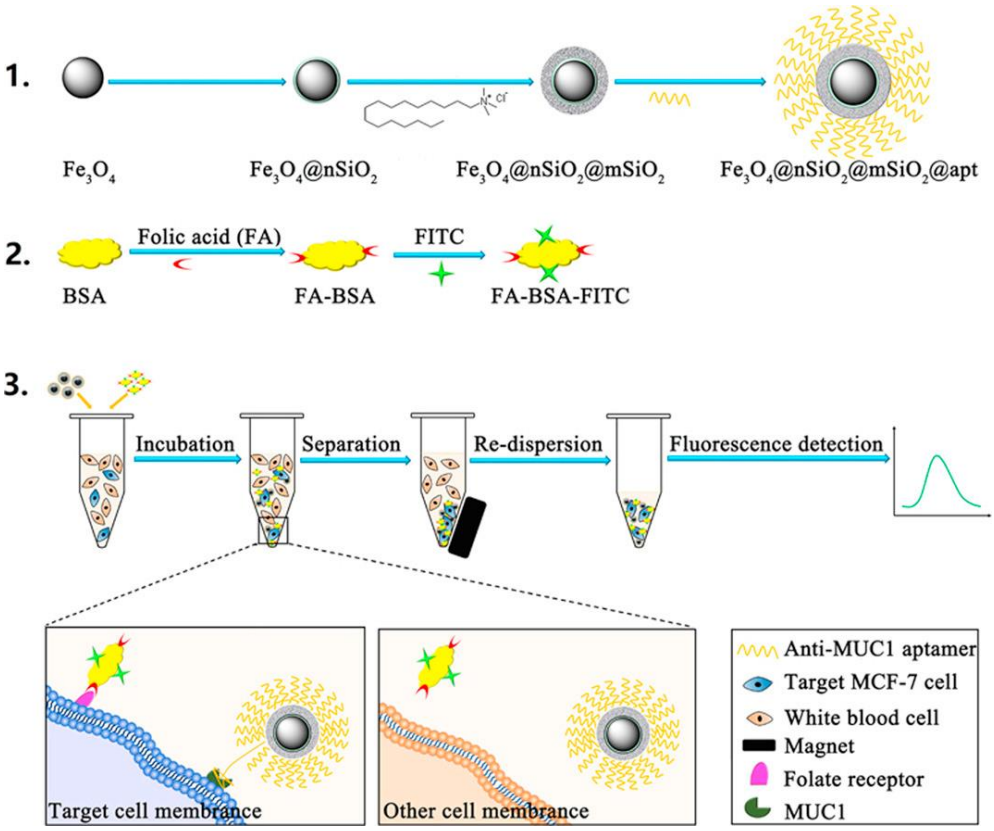

Figure 3. Principle of dual-target recognition sandwich assay for MCF-7 cells detection. Reprinted from reference [66] with permission from Elsevier.

Superparamagnetic-upconversion nanocomposite was also demonstrated for deep tissue imaging and treatment of cancers.[67] Namely, folic acid (FA)-targeted, photosensitizer (PS)-loaded Fe_3O_4@$NaYF_4$:Yb/Er nanocomposites were synthesized for dual imaging capability, fluorescence and T2-weighted MRI, along with the ability for treatment of cancer by photodynamic therapy (PDT) with near-infrared (NIR) irradiation. *In vivo* experiments on mice revealed the efficient capability of PDT with the synthesized nanocomposite to reduce the volume of tumors with preferential accumulation of the nanomedicine in tumor tissues.

Previously, triple-functional core–shell structured nanomaterial $NaGdF_4$:Yb,Er@CaF_2@SiO_2-PS was synthesized and its *in vitro* applicability for PDT, MRI and fluorescence/luminescence

imaging of tumors was demonstrated.[68] Therein, the upconversion nanoparticles $NaGdF_4$:Yb,Er@CaF_2 were first prepared as cores and mesoporous silica shell was then formed, containing covalently attached PSs (silicon phthalocyanine dihydroxide and haematoporphyrin)) for PDT activity. Under excitation at 980 nm, the nanomaterial gives luminescence emissions at 550 and 660 nm. The former is used for fluorescence imaging and the latter is used for energy absorption of PS to generate singlet oxygen and hence PDT. Magnetic measurements revealed that the synthesized material is paramagnetic, attributed to the seven unpaired inner 4f electrons of Gd^{3+} ions. This feature was showcased as applicable for T1-weighted imaging, evidently through penetration of water within the mesopores of the nanotheranostic agent. The constructed $NaGdF_4$:Yb,Er@CaF_2@SiO_2-PS nanomaterial showed similar capability for MRI to Gd–DTPA, which is readily applicable in clinics.

Another type of magnetic-upconverting nanorattle core-shell particles have been demonstrated for efficient application in magnetic field-targeted cancer therapy and imaging *in vivo*.[69] The nanoparticles were composed of upconverting hydrophilic, rare-earth doped $NaYF_4$ shells for imaging, each containing a loose magnetic nanoparticle inside the hollow compartments. Doxorubicin filled nanomaterial was intravenously injected into the tumour-bearing mice while the neodymium disk magnets were located at the tumour site, which benefited in the enhanced efficiency of the drug delivery process and shrinkage of tumor volumes. This study demonstrated a facile methodology for increasing the activity of designed nanotherapeutics through the active magnetic targeting.

Recently an innovative principle for analyte dependent on/off switching of MRI was described.[70] The authors attached a T1 contrast agent (Gd(III) complex) to the surface of silica-embedded superparamagnetic nanoparticles (12nm $Zn_{0.4}Fe_{2.6}O_4$). The distance between Gd(III) and

superparamagnetic nanoparticles was modified by controlling the thickness of the SiO_2 separating layer from 18 to 2 nm. In this system, the superparamagnetic nanoparticles exhibited quenching of T1 weighted MRI in a distance-dependent manner, which was termed as a novel magnetic resonance tuning (MRET) principle between a paramagnetic 'enhancer' and a superparamagnetic 'quencher'. Hence, the intensity of T1 MRI signals increases significantly with increasing the separation from the quencher, which was utilized for sensing specific molecules, by designing H_2O_2 cleavable sulfonate linker or a matrix metalloproteinase-2 (MMP-2) cleavable peptide linker between the enhancer and the quencher. Thus, in the presence of H_2O_2 or MMP-2, cancer biomarker, the T1 MRI signals intensify and allow *in vitro* and *in vivo* cancer tracking.

Novel cobalt oxide nanoprisms containing doxorubicin were recently demonstrated as responsive to intratumoral oxidizing and acidifying environment, with switching the MRI imaging from T2 to T1 and luminescence recovery of doxorubicin.[71] This principle allowed efficient multimodal *in vivo* imaging and simultaneous treatment of cancer. For further studies regarding the applications of magnetic nanomaterials in MRI the focused review articles on this topic should be consulted.[72,73]

4. Magnetic-field responsive therapy and drug delivery

Hyperthermia of cancer through exposure of MNPs to alternating magnetic field (AMF) has been demonstrated in recent years as a particularly promising treatment option. Capability of magnetic nanomaterials to generate heat upon exposure to AMF can be expressed by specific loss power (SLP), which is the value of heat dissipation in water per unit mass of magnetic material. Different iron oxide-based nanoparticles, such as nanocubes,[74,75] nanoparticles with magnetically hard core and magnetically soft shell,[76] and multi-core nanoparticles,[77] have been reported recently with SLP

values of up to 1000 W/g. However, a recent study demonstrated that unprecedented SLP values of up to 5000 W/g can be obtained when cubic MNPs are exposed to near infrared irradiation simultaneously to AMF.[78] This synergistic effect of magnetic hyperthermia and photothermal effects of magnetic nanocubes is demonstrated as very applicable for the treatment of tumors *in vitro* and *in vivo*. Similar effects have been observed in case of multifunctional silver/magnetite nanoflowers (Ag/Fe_3O_4), with the increase in SLP value by an order of magnitude under the application of both an external magnetic field and simultaneous laser irradiation.[79]

MNPs of 11 nm mean diameter with 2000 MW polyethylene (PEG) coating have been showcased to achieve preferential accumulation in tumor tissues,[80] through the EPR effect, which helped in efficient ablation of tumor tissues upon exposure of MNP-treated mice to AMF. The authors demonstrated that much higher temperature was achievable in tumor tissues compared to healthy muscle upon exposure to AMF, which is due to accumulation of the nanoparticles in tumors. Also, the survivability of AMF treated tumor-bearing mice was much higher to the untreated ones. To further increase the efficiency of hyperthermia, more sophisticated and very diverse nanosystems have been reported. Recently, wüstite $Fe_{0.6}Mn_{0.4}O$ nanoflowers have been demonstrated as effective theranostic agents with T_1-T_2 dual-mode magnetic resonance imaging (MRI) capabilities and efficient magnetic hyperthermia treatment ability.[81] *In vitro* and *in vivo* experiments revealed enhanced cancer cell apoptosis and complete tumor regression in mice upon the treatment with the nanoflowers and exposure to alternating magnetic field. Exposure to multiple repeatable magnetic hyperthermia treatments have also shown enhanced therapeutic effect.[82] The authors assembled magnetic nanoparticles within biodegradable poly(organophosphazene) hydrogel nanocapsules, which showed excellent MRI capabilities and induced necrosis of cancer cells *in vivo* after four cycles of exposure to magnetic hyperthermia at mild temperatures, without severe damage on the

surrounding healthy tissues.

Hyperthermia can be used in combination with drug delivery, to facilitate the delivery of the payload from the nanoparticle at the cancer site. J. Liu et al prepared thermo-, glucose- and pH-responsive poly(vinyl alcohol)-*b*-poly(N-vinylcaprolactam)-based nanogels conjugated to 7.5 nm maghemite nanoparticles through boronate linkages.[83] The nanogel was tested with loaded Nil Red as a model hydrophobic drug, and no premature release was noticed in the absence of glucose and at physiologic conditions. The release was triggered upon exposure to glucose or acidic pH, while exposure to AMF was showcased to lead to hyperthermia and enhancement of the dye release. Furthermore the capability of the hybrid material for T2-weighted MRI was demonstrated, as well as the glucose- and acidification-induced toxicity of drug Tamoxifen loaded nanogel against mouse fibroblast-like L929 and human melanoma MEL-5 cell lines. In another study, Park et al. performed the synthesis of Fe-Co core nanoparticles and wrapped them with a graphitic carbon shell (Fe-Co/C).[84] The nanoparticles of 11 nm were coated with dextran for biocompatibility and were modified with antibodies or cyclic RGD peptide to target glioblastoma. The nanoparticles were also applicable for MRI and Raman bimodal imaging, endowing them with theranostic capabilities, as showcased by *in vitro* and *in vivo* experiments. Layer by layer functionalization of the Fe-Co/C nanoparticles was employed for surface modification with PEI and subsequently with siRNA, In vitro experiments were carried out in order to deliver siRNA to glioblastoma U87 cells and effective silencing of oncogenic EGFRvIII gene was demonstrated, as well as the synergistic therapeutic effect of magnetic field-induced hyperthermia. Zn-doped iron oxide nanoparticles of 15.4 nm hydrodynamic diameter were also coated with PEI and then grafted with a pro-apoptotic mitochondria-targeting peptide (ATAP) along with a polyethylene glycol (PEG)-conjugated tumor targeting peptide (iRGD).[85] Both peptides were attached to the nanoparticle's surface through

disulfide linkages and their anticancer effect was showcased on glioblastoma multiforme (U87vIII) and metastatic breast cancer cells ((MDA-MB-231). Magnetic field induced hyperthermia further enhanced cancer cell death through synergistic effect. Preliminary *in vivo* testing was carried out with esophageal cancer xenograft model and showed suppression of tumor growth. Omar et al. prepared large pore (20-60 nm) iron oxide-MSN composites of 100 nm diameter for the delivery of proteins to cancer cells.[86] The nanoparticles were biodegradable and were functionalized with APTES in order to immobilize negatively charged proteins in the pores of the nanoparticles by electrostatic interactions. The model protein was ferritin, which was released in aqueous environment by lowering pH or upon exposure to AMF. The ferritin-loaded nanoparticles were also tested on HeLa cancer cells, and the protein was successfully delivered due to the acidic compartment of lysosomes, as shown by confocal microscopy.

MNPs can cause damage to the cells even without production of heat. For example, exposure to low frequency pulsed magnetic field was observed to cause cell killing through a mechanical damage.[87] Similar mechanical effect on cancer cells was observed in case of the movement of cancer cells-treated MMSN in response to the magnetic pull.[88]

5. Magnetic nanoparticle-polymer core-shell nanotheranostics

Various hybrid materials containing polymers and magnetic nanoparticles are being developed in recent years for battling cancer through different therapeutic and diagnostic methodologies.[89] Complex heat-responsive anticancer nanomedicines can be designed by exploiting the heat-producing feature of magnetic nanoparticles upon exposure to AMF. Core-shell nanoparticles containing magnetite core of 20 nm in diameter, 20 nm-thick mesoporous silica shell and

covalently attached thermo-sensitive polymer, poly[(ethylene glycol)-co-(L-lactide)] (P(EO-co-LLA)) coating, as "gatekeeper" onto the mesopores, have been showcased for efficient simultaneous treatment of cancer by AMF-induced hyperthermia and thermo/pH-responsive drug delivery.[90] *In vitro* studies on HeLa cancer cells revealed that hyperthermia alone causes the decrease in viable cells but it is augmented by the presence of mesopore-loaded drugs which caused killing of cancer cells with increase in temperature or by acidification inside the endosomal compartments. Recently, a sacrificial mesoporous carbon template was employed for the construction of mesoporous iron oxide nanosystem, which was capped with a thermoresponsive polymer shell and entrapping doxorubicin within the material (Figure 4).[91] Gradual release of the drug was observed in acidic environment, which was significantly enhanced upon exposure to alternating magnetic field. Therapeutic effects of the nanosystem were observed on different cancer cells and even treatment resistant cancer cells, while no effect was observed on healthy cells, ascribed to a low internalization of nanoparticles. Combination anticancer effect of magnetic hyperthermia and photodynamic therapy was recently demonstrated by magnetite nanoparticles functionalized with photosensitizer conjugated hyaluronic acid, which showed cooperative inhibition of tumor growth.[92] Capability for dual imaging (optical and MRI) with the same nanomaterial was also demonstrated.

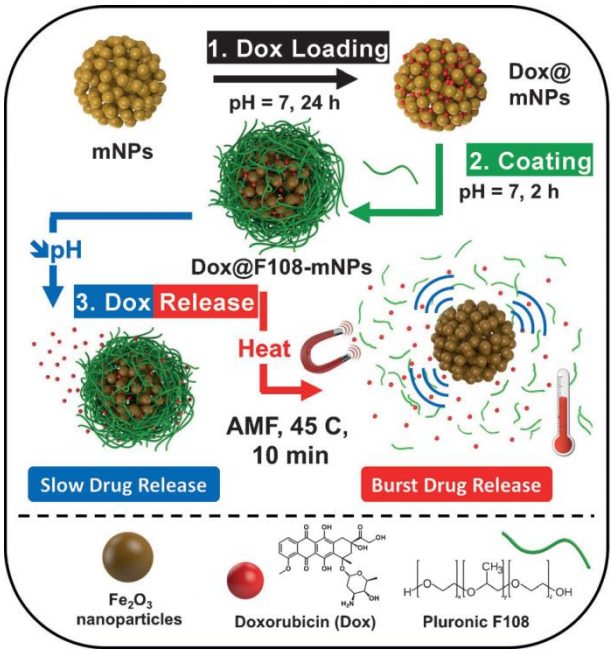

Figure 4. Schematic representation of application of polymer-capped mesoporous iron oxide nanoparticles for loading doxorubicin and its pH-and hyperthermia-responsive release. Reproduced from Ref 91 with permission from Wiley.

Hyaluronic acid-modified Fe_3O_4@Au core/shell nanostars (Fe_3O_4@Au-HA NSs) were also demonstrated for a triple-mode imaging (magnetic resonance (MR), computed tomography (CT), and thermal imaging) with capabilities for photothermal therapy of tumors.[93] Ferritin was showcased as an efficient shell for construction of biocompatible magnetic nanoarchitectures.[94] A series of uniform magnetic/plasmonic Fe_3O_4/Au core/shell nanoparticles with precisely controlled core diameters and shell thicknesses were recently developed by employing amphiphilic star-like P4VP-*b*-P*t*BA-*b*-PEO triblock copolymers as nanoreactors.[95] Core-shell nanostructure consisting of Fe_3O_4 nanoparticles as the core, organic alginate as the shell, and cell-targeting ligands (i.e. D-galactosamine) decorated on the outer surface were reported for targeted treatment of cancer through alternating magnetic field-induced hyperthermia.[96]

A new imaging modality with magnetic nanoparticles, magnetic particle imaging (MPI) was also recently utilized for cancer-cell labeling and *in vivo* tracking, by Janus iron oxide nanoparticles, functionalized with semiconducting polymer.[97] The obtained nanoparticles showed higher efficacy for MPI-*in vivo* particle tracking than commercially available agents and showcased an effective alternative to MRI with high sensitivity, unlimited tissue penetration, linear quantitativity and nearly no background from tissues

.

6. Core-shell silicon-based magnetic cancer nanotheranostics

Nanoparticles based on mesoporous silica are particularly attractive scaffolds for construction of complex nanotherapeutics, due to high surface area, isostructural mesoporosity and a particle diameter (100–200 nm) in the range suitable for exploiting EPR effect of cancerous tissue, to enhance the selectivity of the treatment. Magnetic core/shell analogues of MSN material (MMSN) are readily obtained by including magnetic nanoparticles during the sol-gel surfactant templated synthesis procedure.[98–101] Transmission electron micrographs of some of literature-reported MMSN materials are represented on Figure 5, characterized by various pore and particles morphologies.

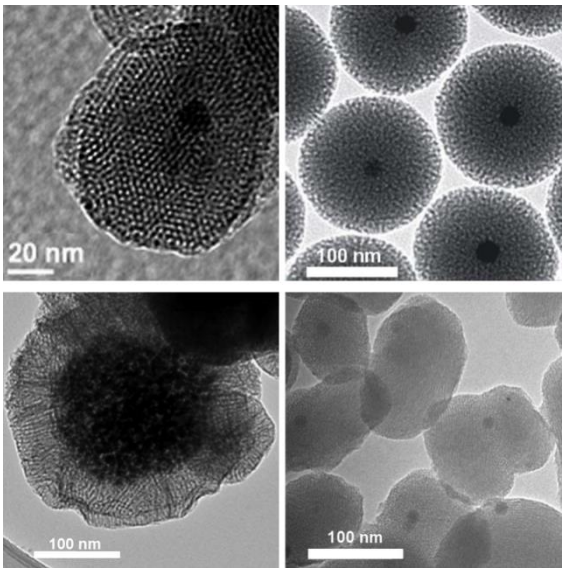

Figure 5. a) Transmission electron micrograph of MMSN materials. Reproduced from literature reports of the authors.[98–101]

Moreover, the functionalization can be selectively applied to different surfaces of MSN, i.e. the external surface can be functionalized with one moiety while the surface inside the mesopores can contain another type of functional groups. This property enables construction of complex nanodevices, with separate functionalized moieties performing different functions simultaneously (evading immune response, selective cancer targeting, on desire-responsiveness of the treatment activity, imaging). Cancer targeting can be enhanced beyond the EPR-related accumulation by attaching cancer specific ligands on the external surface of nanodevices,[102] while at the same time MSN-based nanodevice can contain magnetically active core to produce MMSN (Figure 4.1.c) and to open possibilities for magnetic field targeting.[100,103] Ultimately, the activity of the drug-carrying nanodevice can be designed in such a manner to render them responsive to various intratumoral or to externally applicable stimuli, thus enabling “on desire” drug release from the nanotherapeutic agent.[104]

Capabilities for MRI imaging and drug delivery with MMSN type materials were demonstrated in 2006-2008 by three independent groups. The Mou's group prepared Fe_3O_4@silica core-shell nanoparticles and fused them with FITC-functionalized MSN to prepare Mag-Dye@MSN which were able to act as bimodal imaging probes and drug reservoirs.[105] These nanocomposites, 120 nm in diameter, were used to labeled cells *in vitro* and for *in vivo* tracking experiments.[106] After administration of Mag-Dye@MSN though eye vein injection of mice, the nanoparticles accumulated in the liver and spleen as shown by T2 weighted-MRI and histological sections of tissue organs. An MRI long term tracking (three months) revealed that Mag-Dye@MSN were not easily excreted and were resistant to decomposition. No toxicity or abnormalities were noticed. The Zink's group prepared multifunctional MSN of 100-200 nm diameter encapsulating iron oxide nanocrystal of 20 nm diameter, by aqueous transfer of iron oxide nanocrystals coated with CTAB and by subsequent basic hydrolysis-polycondensation of TEOS in the presence of CTAB. The MMSN were labeled with FITC for fluorescence imaging, coated with phosphonate and folic acid to prevent aggregation and to target cancer cells respectively. MMSN were used for MRI in solution and inside cancer cells, for paclitaxel and camptothecin delivery in cancer cells with significant efficiency.[107]

Hyeon's group independently used similar procedure to synthesize MMSN. The authors showcased EPR-induced accumulation of MMSN nanoparticles in tumor tissues, which resulted in dark areas in T2-weighted images due to the presence of superparamagnetic nanoparticles.[108] Studying relaxivities of core-shell MMSN of different diameters, i.e. different silica shell thicknesses, revealed that r2-relaxivity does not decrease significantly in comparison to the superparamagnetic nanoparticles without mesoporous silica coating up to the particles of 75 nm in diameter.[109] Therefore, mesoporosity of silica shell allows unhindered water penetration into the proximity of superparamagnetic nanoparticles, which allows influence on r2-relaxation. On the

contrary, when non-porous silica shell is grafted on the magnetite core, r2-relaxation decreases rapidly already at the thickness of the shell at 20 nm.[110] In the same study, the authors demonstrated the enhancement of MRI accuracy in case of the presence of T1-contrast agent in addition to the superparamagnetic nanoparticles as T2-contast agents within the same nanoparticle.

Another study reported combination of paramagnetic and superparamagnetic nanomaterials, as T1 and T2 contrast agents, respectively, which is capable to eliminate false errors (artifacts) from the raw images to enhance accuracy of the MRI.[111] This effect is achieved through the capability to perform "AND logic gate" algorithm, with the contribution of filtering effect. The constructed artifact filtering imaging agents (AFIAs) have core-shell structure, containing different superparamagnetic nanoparticles as T2 contrast agent in the core, SiO_2 as the separating layer and various paramagnetic material as the shell and T1 contrast agent, as represented on the Figure 6. The authors showcase that the thickness of the separation layer of 16 nm is suitable to have both T1 and T2 signals of high magnitude at the same time and demonstrate the efficacy of constructed AFIAs for artifact-free imaging by *in vitro* and *in vivo* experiments.

Synthesis and biomedical applications of different MMSN materials was reviewed in depth in 2013,[112] however many attractive important achievements on this topic have been published since. Synergic effect between the intracellular hyperthermia and chemotherapy triggered by exposure to AMF was recently demonstrated by *in vivo* experiments.[113] The authors utilized MMSN material containing core magnetite and drug loaded mesopores, entrapped by the presence of temperature-responsive polymer as the gatekeeper. The analogues of MMSN material with radial porosity and surface-attached folic acid were also demonstrated, both *in vitro* and *in vivo*, for AMF-responsive hyperthermia and simultaneous MRI-guided and AMF-responsive chemotherapy for breast cancer.[114]

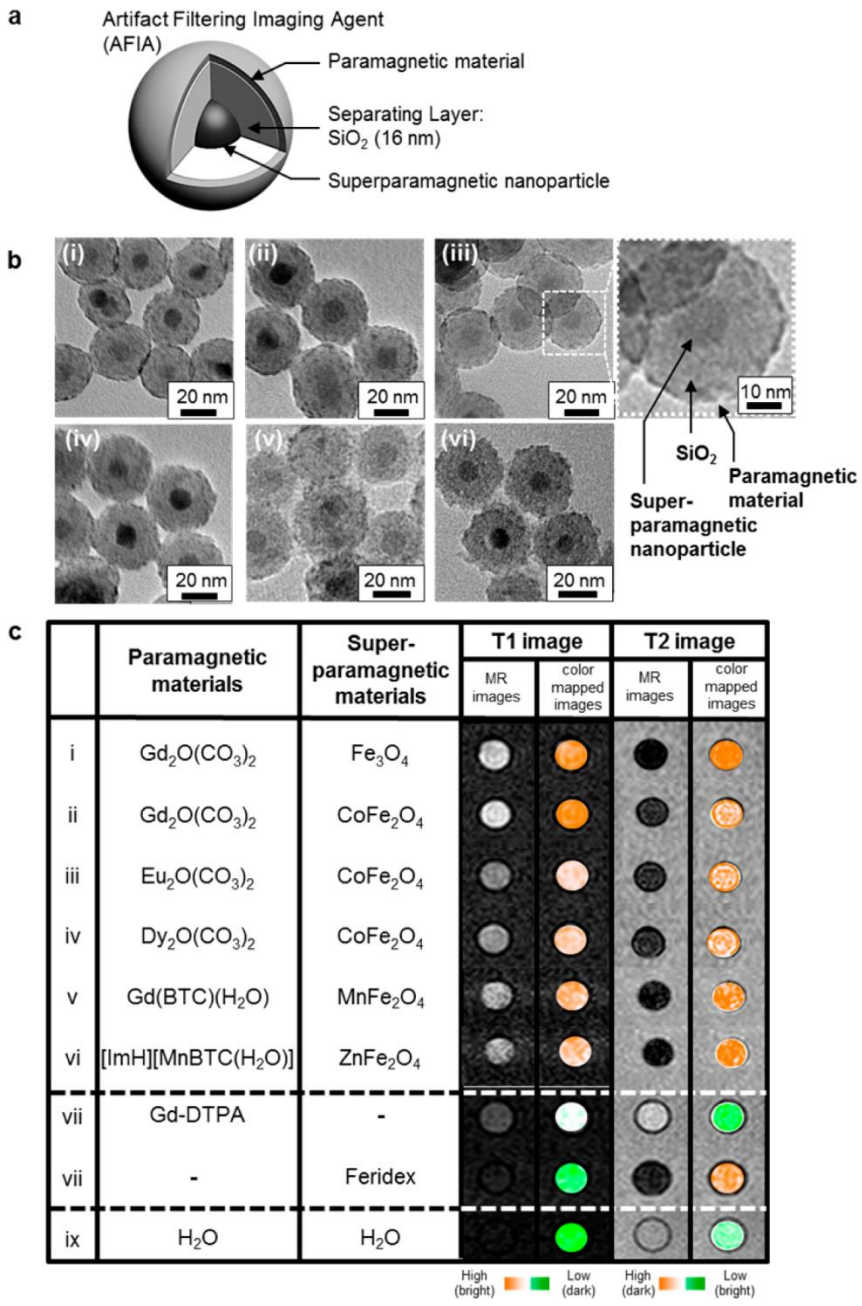

Figure 6. Variety of AFIAs and their MRI contrast effects. (a) Schematic illustration of core-shell structured AFIA. (b) TEM images of various core-shell structured AFIAs and (c) MRI images and their color-coded images of AFIAs and conventional contrast agents. Reprinted from Ref 111 with permission from. Copyright 2014 American Chemical Society.

Vascular endothelial growth factor (VEGF)-small interfering RNA (siRNA) was encapsulated into

a MMSN-based, polyethylenimine (PEI)-capped, polyethylene glycol (PEG)-grafted, fusogenic peptide (KALA)-functionalized siRNA delivery system, which showed significant effectiveness with regard to VEGF gene silencing *in vitro* and *in vivo*, yielding an efficient antiangiogenesis effect on ovarian cancer tissues.[115]

More recent study showed application of complex MMSN nanoarchitectures for *in vivo* MRI imaging and precise therapy.[116] In this study doxorubicin was loaded inside the mesopores of MMSN and β-cyclodextrin (β-CD) was used as the gatekeeper, which was linked to the pore entrances through a platinum(IV) prodrug. In addition, adamantane-PEG8-glycine-arginine-glycineaspartic-serine (AD-PEG_8-GRGDS) was functionalized on MMSN through the strong AD-β-CD host-guest interaction, for additional targeting of cancer by binding to cancer-overxpressed $\alpha_v\beta_3$ integrin. The functioning principle of this nanomedicine is that the drug delivery is intracellularly activated by reduction of Pt(IV) to the toxic platinum(II) drug. The authors showcased that the material efficiently reduced the volume of cancer tissue *in vivo* and that magnetic targeting is an effective method for increasing the accumulation of MMSN in cancer tissue and to enhance the therapeutic effect.

In another study, J.Li and co-workers coated MMSN with red blood cell membrane (RBC@MMSN).[117] Photosensitizer hypocrellin A was adsorbed inside the mesoporous structure. In vivo experiments after tail vein injection of RBC@MMSN in tumor-xenografted mice demonstrated long circulation time and stealth behavior of RBC@MMSN. Magnetic targeting allowed accumulation of RBC@MMSN in the tumor and light irradiation led to efficient photodynamic therapy with necrosis of cancer tissues showing the efficiency of RBC@MMSN.

Novel multifunctional MMSN type of material was reported containing magnetite and gold

nanoparticles as the core and photosensitizer chlorin e6 (Ce6) and doxorubicin inside the mesopores of mesoporous silica shell (Figure 7).[118] These molecules were entrapped by layer-by-layer assembly of alginate and chitosan as pH-sensitive gatekeepers with the final layer containing small hairpin RNA (shRNA) which downregulates P-glycoprotein (P-gp), protein involved in drug efflux and contributes to occurrence of treatment resistance. Real-time imaging-guided simultaneous PDT therapy, chemotherapy and gene therapy was enabled *in vivo* by the presence of iron oxide and Au nanoparticles for MRI and CT imaging, with efficient combination of PDT and chemotherapy through overcoming multidrug resistance by simultaneous gene silencing.

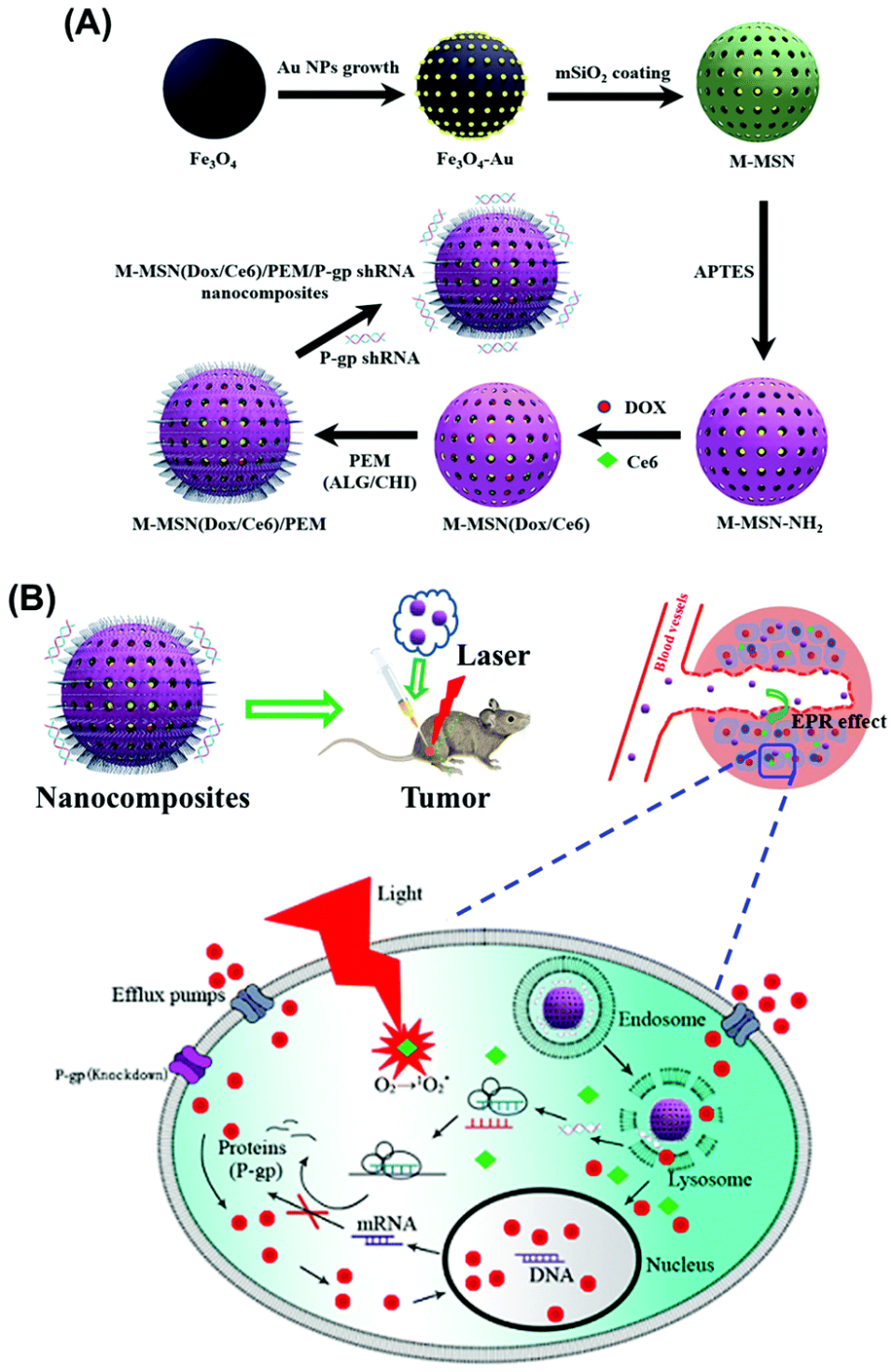

Figure 5. Schematic illustration of the preparation process of MMSN(Dox/ Ce6)/PEM/P-gp shRNA nanocomposites (A) and intracellular pH-triggered release in the tumor cells (B). Reproduced from Ref. 118 with permission from The Royal Society of Chemistry.

7. Perspectives

Magnetic nanomaterials and complex magnetic nanoarchitectures have indeed bright prospect regarding their possibilities for biomedical applications. Superparamagnetic iron oxide nanoparticles (SPION) are already showing high potential for application in clinics for magnetic resonance imaging and magnetic hyperthermia of cancer.[119] Novel research studies discover a plethora of possible complex designs of magnetic nanomaterials, with magnetic nanoparticles forming the core and the shell consisting of polymers, surfactants or mesoporous silica. These nanomaterials showcase significantly enhanced therapeutic and imaging capabilities compared to SPION. The shell, therefore, brings additional features to the magnetic nanomaterial with tunable morphology and porosity, which is typically reflected in embedding drugs, imaging agents or genes[120] within their framework and possibilities for surface functionalization with additional therapeutic, and targeting ligands. Hence, highly selective multi-functionalized nanotherapeutics can be constructed, capable of utilizing magnetic field and/or ligands for homing the drug loaded nanocarriers to the therapeutic area, along with possibilities for magnetic hyperthermia treatment of the ill tissues and live monitoring of the treatment through magnetic resonance or/and other types of imaging. In addition, sensing of cancer-related biomolecules (cancer biomarkers) and imaging of tumor microenvironment is a promising methodology for enabling early and accurate detection of cancer,[121] as well as for obtaining information about the responses, mechanisms, and efficacy of the nanotherapeutics, which is of paramount importance for treatment optimization and obtaining personalized nanomedicines. These types of versatile multifunctional nanomaterials, combining sensing, imaging and therapy within one nanotheraputic agent, could be the future of clinical procedures, though their complexity brings concerns regarding the adverse effects on

healthy tissues. Particularly the degradability,[122] pharmacology-biodistribution, elimination and excretion of these nanomaterials need to be thoroughly addressed for designing novel clinically applicable nanotherapeutics.

Acknowledgments

For financial support, NK is thankful to the Ministry of Science and Technological Development of the Republic of Serbia (Grant no. III44006). The PHC grant Pavle Savic N° 40800RD (451-03-01963/2017-09/05) is gratefully acknowledged.

References

1 S. Hoelder, P. A. Clarke and P. Workman, *Mol. Oncol.*, 2012, **6**, 155–176.

2 M. Marković, N. Knezević, M. Momcilović, S. Grgurić-Sipka, L. Harhaji, V. Trajković, M. Mostarica Stojković, T. Sabo and D. Miljković, *Eur. J. Pharmacol.*, 2005, **517**, 28–34.

3 N. Ž. Knežević and J.-O. Durand, *Chempluschem*, 2015, **80**, 26–36.

4 K. Greish, *J. Drug Target.*, 2007, **15**, 457–464.

5 A. K. Gupta and M. Gupta, *Biomaterials*, 2005, **26**, 3995–4021.

6 R. A. Revia and M. Zhang, *Mater. Today*, 2016, **19**, 157–168.

7 M. Wankhede, A. Bouras, M. Kaluzova and C. G. Hadjipanayis, *Expert Rev. Clin. Pharmacol.*, 2012, **5**, 173–186.

8 M. Magro, D. Baratella, E. Bonaiuto, J. de A Roger and F. Vianello, *Curr. Med. Chem.*, 2018, **25**, 540–555.

9 S. Serres, M. S. Soto, A. Hamilton, M. A. McAteer, W. S. Carbonell, M. D. Robson, O. Ansorge, A. Khrapitchev, C. Bristow, L. Balathasan, T. Weissensteiner, D. C. Anthony, R. P. Choudhury, R. J. Muschel and N. R. Sibson, *Proc. Natl. Acad. Sci. U. S. A.*, 2012, **109**, 6674–667

10 K. Turcheniuk, A. V Tarasevych, V. P. Kukhar, R. Boukherroub and S. Szunerits, *Nanoscale*, 2013, **5**, 10729–10752.

11 D. Ling, N. Lee and T. Hyeon, *Acc. Chem. Res.*, 2015, **48**, 1276–1285.

12 S. Laurent, D. Forge, M. Port, A. Roch, C. Robic, L. Vander Elst and R. N. Muller, *Chem. Rev.*, 2008,

108, 2064–2110.

13 A. Malik, T. Tahir Butt, S. Zahid, F. Zahid, S. Waquar, M. Rasool, M. H. Qazi and A. M. Qazi, *J. Nanotechnol.*, 2017, **2017**, 8.

14 D. Yoo, J.-H. Lee, T.-H. Shin and J. Cheon, *Acc. Chem. Res.*, 2011, **44**, 863–874.

15 M. Angelakeris, *Biochim. Biophys. Acta*, 2017, **1861**, 1642–1651.

16 G. Kandasamy and D. Maity, *Int. J. Pharm.*, 2015, **496**, 191–218.

17 M. K. Lima-Tenório, E. A. Gómez Pineda, N. M. Ahmad, H. Fessi and A. Elaissari, *Int. J. Pharm.*, 2015, **493**, 313–327.

18 R. A. Revia and M. Zhang, *Mater. Today (Kidlington).*, 2016, **19**, 157–168.

19 O. L. Gobbo, K. Sjaastad, M. W. Radomski, Y. Volkov and A. Prina-Mello, *Theranostics*, 2015, **5**, 1249–1263.

20 A. J. Cole, V. C. Yang and A. E. David, *Trends Biotechnol.*, 2011, **29**, 323–332.

21 J. E. Lee, N. Lee, T. Kim, J. Kim and T. Hyeon, *Acc. Chem. Res.*, 2011, **44**, 893–902.

22 Y. Wang and H. Gu, *Adv. Mater.*, 2015, **27**, 576–585.

23 R. A. Bini, R. Fernando, C. Marques, F. J. Santos, J. A. Chaker and M. Jafelicci, *J. Magn. Magn. Mater.*, 2012, **324**, 534–539.

24 Z. Guo, T. Pereira, O. Choi, Y. Wang and H. T. Hahn, *J. Mater. Chem.*, 2006, **16**, 2800–2808.

25 J. Zhao, M. Milanova, M. M. C. G. Warmoeskerken and V. Dutschk, *Colloids Surfaces A Physicochem. Eng. Asp.*, 2012, **413**, 273–279.

26 N. Ž. Knežević and J.-O. Durand, *Chempluschem*, 2015, **80**, 26–36.

27 C. M. Blumenfeld, M. D. Schulz, M. S. Aboian, M. W. Wilson, T. Moore, S. W. Hetts and R. H. Grubbs, *Nat. Commun.*, 2018, **9**, 7.

28 M. Radović, M. P. Calatayud, G. F. Goya, M. R. Ibarra, B. Antić, V. Spasojević, N. Nikolić, D. Janković, M. Mirković and S. Vranješ-Đurić, *J. Biomed. Mater. Res. Part A*, 2015, **103**, 126–134.

29 D. Benedetto, F. Benyettou and Y. Lalatonne, *Phys. Chem. Chem. Phys.*, 2011, **13**, 10020–10027.

30 A. Bahrami, T. Vincent, A. Garnier, F. Larachi, J. Boukouvalas and M. C. Iliuta, *Ind. Eng. Chem. Res.*, 2017, **56**, 10981–10989.

31 C. Tudisco, A. L. Pellegrino, G. Malandrino and G. G. Condorelli, *Surf. Coatings Technol.*, 2018, **343**, 75–82.

32 G. Hemery, C. Genevois, F. Couillaud, S. Lacomme, E. Gontier, E. Ibarboure, S. Lecommandoux, E. Garanger and O. Sandre, *Mol. Syst. Des. Eng.*, 2017, **2**, 629–639.

33 E. Perillo, K. Hervé-Aubert, E. Allard-Vannier, A. Falanga, S. Galdiero and I. Chourpa, *J. Colloid*

Interface Sci., 2017, **499**, 209–217.

34 R. Massart, *IEEE Trans. Magn.*, 1981, **17**, 1247–1248.

35 C. Tudisco, M. T. Cambria, A. E. Giuffrida, F. Sinatra, C. D. Anfuso, G. Lupo, N. Caporarello, A. Fa1langa, S. Galdiero, V. Oliveri, C. Satriano and G. G. Condorelli, *Nanoscale Res. Lett.*, , DOI:10.1186/s11671-018-2459-8.

36 M. Radović, M. Mirković, M. Perić, D. Janković, A. Vukadinović, D. Stanković, Đ. Petrović, M. Bošković, B. Antić, M. Marković and S. Vranješ-Đurić, *J. Mater. Chem. B*, 2017, **5**, 8738–8747.

37 H. Chen, X. Li, F. Liu, H. Zhang and Z. Wang, *Mol. Pharm.*, 2017, **14**, 3134–3141.

38 L. Lartigue, C. Innocenti, T. Kalaivani, A. Awwad, M. del M. Sanchez Duque, Y. Guari, J. Larionova, C. Guérin, J.-L. G. Montero, V. Barragan-Montero, P. Arosio, A. Lascialfari, D. Gatteschi and C. Sangregorio, *J. Am. Chem. Soc.*, 2011, **133**, 10459–10472.

39 K. Gharbi, F. Salles, P. Mathieu, C. Amiens, V. Collière, Y. Coppel, K. Philippot, L. Fontaine, V. Montembault, L. S. Smiri and D. Ciuculescu-Pradines, *New J. Chem.*, 2017, **41**, 11898–11905.

40 C. Bordeianu, A. Parat, C. Affolter-Zbaraszczuk, R. N. Muller, S. Boutry, S. Begin-Colin, F. Meyer, S. Laurent and D. Felder-Flesch, *J. Mater. Chem. B*, 2017, **5**, 5152–5164.

41 C. Linot, J. Poly, J. Boucard, D. Pouliquen, S. Nedellec, P. Hulin, N. Marec, P. Arosio, A. Lascialfari, A. Guerrini, C. Sangregorio, M. Lecouvey, L. Lartigue, C. Blanquart and E. Ishow, *ACS Appl. Mater. Interfaces*, 2017, **9**, 14242–14257.

42 D. Peddis, F. Orrù, A. Ardu, C. Cannas, A. Musinu and G. Piccaluga, *Chem. Mater.*, 2012, **24**, 1062–1071.

43 Y. Tanaka, S. Saita and S. Maenosono, *Appl. Phys. Lett.*, 2008, **92**, 7.

44 J. Salafranca, J. Gazquez, N. Pérez, A. Labarta, S. T. Pantelides, S. J. Pennycook, X. Batlle and M. Varela, *Nano Lett.*, 2012, **12**, 2499–503.

45 N. Ž. Knežević, L. Raehm and J.-O. Durand, *Bionanocomposites*, 2017.

46 L. Adumeau, M.-H. Delville and S. Mornet, in *Clinical Applications of Magnetic Nanoparticles From Fabrication to Clinical Applications*, ed. N. T. Thanh, CRC Press, 2018, p. 20.

47 T. Kang, F. Li, S. Baik, W. Shao, D. Ling and T. Hyeon, *Biomaterials*, 2017, **136**, 98–114.

48 J. Huang, Y. Li, A. Orza, Q. Lu, P. Guo, L. Wang, L. Yang and H. Mao, *Adv. Funct. Mater.*, 2016, **26**, 3818–3836.

49 S.-H. Liao, H.-S. Huang, J.-H. Chen, Y.-K. Su and Y.-F. Tong, *RSC Adv.*, 2018, **8**, 4057–4062.

50 X. Wang, B. Li, R. Li, Y. Yang, H. Zhang, B. Tian, L. Cui, H. Weng and F. Wei, *Sensors Actuators B Chem.*, 2018, **255**, 3447–3457.

51 G. Kokkinis, S. Cardoso, F. Keplinger and I. Giouroudi, *Sensors Actuators B Chem.*, 2017, **241**, 438–445.

52 Z. Liu, Y. Liu, S. Shen and D. Wu, *J. Mater. Chem. B*, 2018, **6**, 366–380.

53 S. Fathi Karkan, M. Mohammadhosseini, Y. Panahi, M. Milani, N. Zarghami, A. Akbarzadeh, E. Abasi, A. Hosseini and S. Davaran, *Artif. Cells, Nanomedicine, Biotechnol.*, 2017, **45**, 1–5.

54 I. Giouroudi and E. Hristoforou, *J. Appl. Phys.*, 2018, **124**, 30902.

55 S. L. Znoyko, A. V Orlov, A. V Pushkarev, E. N. Mochalova, N. V Guteneva, A. V Lunin, M. P. Nikitin and P. I. Nikitin, *Anal. Chim. Acta*, 2018, **1034**, 161–167.

56 V. O. Shipunova, M. P. Nikitin, P. I. Nikitin and S. M. Deyev, *Nanoscale*, 2016, **8**, 12764–12772.

57 M. P. Nikitin, A. V Orlov, S. L. Znoyko, V. A. Bragina, B. G. Gorshkov, T. I. Ksenevich, V. R. Cherkasov and P. I. Nikitin, *J. Magn. Magn. Mater.*, 2018, **459**, 260–264.

58 J. Nebu, J. S. Anjali Devi, R. S. Aparna, K. Abha and G. Sony, *Sensors Actuators B Chem.*, 2018, **257**, 1035–1043.

59 A. V Sheahan, A. V Biankin, C. R. Parish and L. M. Khachigian, *Oncotarget*, 2018, **9**, 21613–21627.

60 D. Chen, B. Li, S. Cai, P. Wang, S. Peng, Y. Sheng, Y. He, Y. Gu and H. Chen, *Biomaterials*, 2016, **100**, 1–16.

61 B. Tian, Y. Han, E. Wetterskog, M. Donolato, M. F. Hansen, P. Svedlindh and M. Stromberg, *ACS sensors*, 2018, **3**, 1884-1891

62 M. A. Macha, P. Seshacharyulu, S. R. Krishn, P. Pai, S. Rachagani, M. Jain and S. K. Batra, *Curr. Pharm. Des.*, 2014, **20**, 5287–5297.

63 L. H. Tan, H. Xing and Y. Lu, *Acc. Chem. Res.*, 2014, **47**, 1881–1890.

64 I. Willner, B. Shlyahovsky, M. Zayats and B. Willner, *Chem. Soc. Rev.*, 2008, **37**, 1153–1165.

65 E. Mokany, S. M. Bone, P. E. Young, T. B. Doan and A. V Todd, *J. Am. Chem. Soc.*, 2010, **132**, 1051–1059.

66 W. Wang, S. Liu, C. Li, Y. Wang and C. Yan, *Talanta*, 2018, **182**, 306–313.

67 L. Zeng, L. Luo, Y. Pan, S. Luo, G. Lu and A. Wu, *Nanoscale*, 2015, **7**, 8946–8954.

68 C.-H. Y. Xiao-Fei Qiao, Jia-Cai Zhou, Jia-Wen Xiao, Ye-Fu Wang, Ling-Dong Sun, *Nanoscale*, 2012, **4**, 4611–4623.

69 F. Zhang, G. B. Braun, A. Pallaoro, Y. Zhang, Y. Shi, D. Cui, M. Moskovits, D. Zhao and G. D. Stucky, *Nano Lett.*, 2012, **12**, 61–67.

70 J. Choi, S. Kim, D. Yoo, T.-H. Shin, H. Kim, M. D. Gomes, S. H. Kim, A. Pines and J. Cheon, *Nat. Mater.*, 2017, **16**, 537.

71 Y. Liu, Q. Jia, Q. Guo, W. Wei and J. Zhou, *Biomaterials*, 2018, **180**, 104–116.

72 J. Huang, X. Zhong, L. Wang, L. Yang and H. Mao, *Theranostics*, 2012, **2**, 86–102.

73 Z. Shen, A. Wu and X. Chen, *Mol. Pharm.*, 2017, **14**, 1352–1364.

74 P. Guardia, R. Di Corato, L. Lartigue, C. Wilhelm, A. Espinosa, M. Garcia-hernandez, F. Gazeau, L. Manna and T. Pellegrino, *ACS Nano*, 2012, 3080–3091.

75 C. Martinez-boubeta, K. Simeonidis, A. Makridis, M. Angelakeris, D. Serantes, D. Baldomir, Z. Saghi and P. A. Midgley, *Sci. Rep.*, 2013, **3**, 10.1038/srep01652.

76 J.-H. Lee, J.-T. Jang, J.-S. Choi, S. H. Moon, S.-H. Noh, J.-W. Kim, J.-G. Kim, I.-S. Kim, K. I. Park and J. Cheon, *Nat. Nanotechnol.*, 2011, **6**, 418–22.

77 P. Hugounenq, D. Alloyeau, S. P. Clarke, M. Le, R. Bazzi, D. F. Brougham, C. Wilhelm and F. Gazeau, *ACS Nano*, 2012, 10935–10949.

78 A. Espinosa, R. Di Corato, J. Kolosnjaj-Tabi, P. Flaud, T. Pellegrino and C. Wilhelm, *ACS Nano*, 2016, **10**, 2436–2446.

79 R. Das, N. Rinaldi-Montes, J. Alonso, Z. Amghouz, E. Garaio, J. A. García, P. Gorria, J. A. Blanco, M. H. Phan and H. Srikanth, *ACS Appl. Mater. Interfaces*, 2016, **8**, 25162–25169.

80 H. S. Huang and J. F. Hainfeld, *Int. J. Nanomedicine*, 2013, **8**, 2521–2532.

81 X. L. Liu, C. T. Ng, P. Chandrasekharan, H. T. Yang, L. Y. Zhao, E. Peng, Y. B. Lv, W. Xiao, J. Fang, J. B. Yi, H. Zhang, K.-H. Chuang, B. H. Bay, J. Ding and H. M. Fan, *Adv. Healthc. Mater.*, 2016, **5**, 2092–2104.

82 Z.-Q. Zhang and S.-C. Song, *Biomaterials*, 2016, **106**, 13–23.

83 J. Liu, C. Detrembleur, A. Debuigne, M.-C. De Pauw-Gillet, S. Mornet, L. Vander Elst, S. Laurent, E. Duguet and C. Jérôme, *J. Mater. Chem. B*, 2014, **2**, 1009–1023.

84 J. K. Park, J. Jung, P. Subramaniam, B. P. Shah, C. Kim, J. K. Lee, J.-H. Cho, C. Lee and K.-B. Lee, *Small*, 2011, **7**, 1647–1652.

85 B. P. Shah, N. Pasquale, G. De, T. Tan, J. Ma and K.-B. Lee, *ACS Nano*, 2014, **8**, 9379–9387.

86 H. Omar, J. G. Croissant, K. Alamoudi, S. Alsaiari, I. Alradwan, M. A. Majrashi, D. H. Anjum, P. Martins, R. Laamarti, J. Eppinger, B. Moosa, A. Almalik and N. M. Khashab, *J. Control. Release*, 2017, **259**, 187–194.

87 S. Hapuarachchige, Y. Kato, E. J. Ngen and B. Smith, *PLoS One*, 2016, DOI:10.1371/journal.pone.0156294.

88 N. Ž. Knežević, *J. Nanosci. Nanotechnol.*, 2016, **16**, 4195–4199.

89 A. M. Bonilla and P. H. Gonzalez, *Curr. Pharm. Des.*, 2017, **23**, 5392–5402.

90 W. Guo, C. Yang, H. Lin and F. Qu, *Dalt. Trans.*, 2014, **43**, 18056–18065.

91 F. Benyettou, A. Ocadiz, F. Ravaux, R. Rezgui, M. Jouiad, S. I. Nehme, K. Parsapur and J. Olsen, *Chem. - A Eur. J.*, 2016, **22**, 17020–17028.

92 K. S. Kim, J. Kim, J. Y. Lee, S. Matsuda, S. Hideshima, Y. Mori, T. Osaka and K. Na, *Nanoscale*, 2016,

8, 11625–11634.

93 J. Li, Y. Hu, J. Yang, P. Wei, W. Sun, M. Shen, G. Zhang and X. Shi, *Biomaterials*, 2015, **38**, 10–21.

94 E. Fantechi, C. Innocenti, M. Zanardelli, M. Fittipaldi, E. Falvo, M. Carbo, V. Shullani, L. Di, C. Mannelli, C. Ghelardini, A. M. Ferretti, A. Ponti, C. Sangregorio, P. Ceci, B. Sez, V. Pieraccini, I.-S. Fiorentino, C. Nazionale, C. Golgi, I.- Milano, L. Nanotecnologie and T. Molecolari, *ACS Nano*, 2014, **5**, 4705–4719.

95 D. Yang, X. Pang, Y. He, Y. Wang, G. Chen, W. Wang and Z. Lin, *Angew. chemie*, 2015, **127**, 12259–12264.

96 S.-H. Liao, C.-H. Liu, B. P. Bastakoti, N. Suzuki, Y. Chang, Y. Yamauchi, F.-H. Lin and K. C.-W. Wu, *Int. J. Nanomedicine*, 2015, **10**, 3315–3328.

97 G. Song, M. Chen, Y. Zhang, L. Cui, H. Qu, X. Zheng, M. Wintermark, Z. Liu and J. Rao, *Nano Lett.*, 2018, **18**, 182–189.

98 N. Ž. Knežević, I. I. Slowing and V. S.-Y. Lin, *Chempluschem*, , DOI:10.1002/cplu.201100026.

99 S. Dib, M. Boufatit, S. Chelouaou, F. Sadi-Hassaine, J. Croissant, J. Long, L. Raehm, C. Charnay and J.-O. Durand, *RSC Adv.*, 2014, **4**, 24838–24841.

100 N. Knezevic, *Process. Appl. Ceram.*, 2014, **8**, 109–112.

101 N. Z. Knezevic, C. Mauriello Jimenez, M. Albino, A. Vukadinovic, A. Mrakovic, E. Illes, D. Janackovic, J.-O. Durand, C. Sangregorio and D. Peddis, *MRS Adv.*, 2017, 1–9.

102 N. Ž. Knežević, J. Mrđanović, I. Borišev, S. Milenković, Đ. Janaćković, F. Cunin and A. Djordjevic, *RSC Adv.*, 2016, **6**, 7061–7065.

103 N. Z. Knezevic, I. I. Slowing and V. S.-Y. Lin, *Chempluschem*, 2012, **77**, 48–55.

104 N. Z. Knezevic, *RSC Adv.*, 2013, **3**, 19388–19392.

105 Y.-S. Lin, S.-H. Wu, Y. Hung, Y.-H. Chou, C. Chang, M.-L. Lin, C.-P. Tsai and C.-Y. Mou, *Chem. Mater.*, 2006, **18**, 5170–5172.

106 S.-H. Wu, Y.-S. Lin, Y. Hung, Y.-H. Chou, Y.-H. Hsu, C. Chang and C.-Y. Mou, *Chembiochem*, 2008, **9**, 53–57.

107 M. Liong, J. Lu, M. Kovochich, T. Xia, S. G. Ruehm, A. E. Nel, F. Tamanoi and J. I. Zink, *ACS Nano*, 2008, **2**, 889–896.

108 J. Kim, H. S. Kim, N. Lee, T. Kim, H. Kim, T. Yu, I. C. Song, W. K. Moon and T. Hyeon, *Angew. Chem. Int. Ed. Engl.*, 2008, **47**, 8438–8441.

109 F. Ye, S. Laurent, A. Fornara, L. Astol, J. Qin, A. Roch, A. Martini, M. S. Toprak, R. N. Muller and M. Muhammed, *Contrast Media Mol. Imaging*, 2012, **7**, 460–468.

110 J. S. Choi, J. H. Lee, T. H. Shin, H. T. Song, E. Y. Kim and J. Cheon, *J. Am. Chem. Soc.*, 2010, **132**, 11015–11017.

111 T. Shin, J. Choi, S. Yun, I. Kim, H. Song and Y. Kim, *ACS Nano*, 2014, **8**, 3393–3401.

112 N. Ž. Knežević, E. Ruiz-Hernández, W. E. Hennink and M. Vallet-Regí, *RSC Adv.*, 2013, **3**, 9584.

113 E. Guisasola, L. Asín, L. Beola, J. M. de la Fuente, A. Baeza and M. Vallet-Regí, *ACS Appl. Mater. Interfaces*, 2018, **10**, 12518–12525.

114 Q. Gao, W. Xie, Y. Wang, D. Wang, Z. Guo, F. Gao, L. Zhao and Q. Cai, *RSC Adv.*, 2018, **8**, 4321–4328.

115 Y. Chen, X. Wang, D. S. Zhang and H. Gu, *Int. J. Nanomedicine*, 2015, **10**, 2579–2594.

116 W. Chen, G. Luo, Q. Lei, F. Cao, J. Fan and W. Qiu, *Biomaterials*, 2016, **76**, 87–101.

117 M. Xuan, J. Shao, J. Zhao, Q. Li, L. Dai and J. Li, *Angew. Chemie Int. Ed.*, 2018, **57**, 6049–6053.

118 H. Yang, Y. Chen, Z. Chen, Y. Geng, X. Xie, X. Shen, T. Li, S. Li, C. Wu and Y. Liu, *Biomater. Sci.*, 2017, **5**, 1001–1013.

119 F. K. H. van Landeghem, K. Maier-Hauff, A. Jordan, K.-T. Hoffmann, U. Gneveckow, R. Scholz, B. Thiesen, W. Brück and A. von Deimling, *Biomaterials*, 2009, **30**, 52–57.

120 J. Liu, B. Wang, S. Budi Hartono, T. Liu, P. Kantharidis, A. P. J. Middelberg, G. Q. (Max) Lu, L. He and S. Z. Qiao, *Biomaterials*, 2012, **33**, 970–978.

121 Z. Zhou and Z.-R. Lu, *Adv. Drug Deliver. Rev.*, 2017, **113**, 24–48.

122 J. G. Croissant, Y. Fatieiev and N. M. Khashab, *Adv. Mater.*, 2017, **29**, 1604634.